Available online at www.sciencedirect.com
SCIENCE DIRECT
Journal of Geodynamics 40 (2005) 216–234
JOURNAL OF GEODYNAMICS
http://www.elsevier.com/locate/jog

Fracturing patterns, stress fields and earthquakes in the Southern Dead Sea rift

Oxana V. Lunina [a,*], Yossi Mart [b], Andrei S. Gladkov [a]

[a] *Institute of the Earth's crust, SB RAS, 128 Lermontova st., 664033 Irkutsk, Russia*
[b] *Institute for Marine Studies, University of Haifa, Mt. Carmel, Haifa 31905, Israel*

Received 10 December 2004; received in revised form 16 May 2005; accepted 18 July 2005

Abstract

Integrated investigations including the structural analysis of shear fractures and fault zones, the reconstruction of stress fields and the fractal analysis of the epicentral field of recent earthquakes have been pursued in the Dead Sea rift. The N–S and NW–SE trending faults are very extensive and they display large zones of crushed rock compared with faults of other orientations. According to the fractal analysis of the seismicity over the period of 1983–2002 and a review of historical destructive earthquakes associated with faulting of archaeological sites, large N–S and NW–SE fault zones traced in different sites are the major structures that control the seismic activity in the southern part of the rift. Many of the N–S trending faults are well pronounced within the basins but they are not as frequent in the inter-basin link zones. Meso-structural features document normal fault displacements along the major faults within basins. In the uplifted inter-basin links the kinematics varies from normal to strike-slip faulting along the same fault zones. The NW–SE faults are characterized by normal and oblique displacement, the E–W faults by strike-slip displacements and the NE–SW faults by composite strike-slip and normal displacement. The tectonic stress fields reconstructed from shear fractures orientations show that two main types of local stress tensors are associated with the structural development of the Dead Sea rift: (1) tension with E–W (mainly) and ENE–WSW trending σ_3 and (2) transcurrent with NE–SW (sometimes nearly E–W) trending σ_3 and NW–SE (sometimes nearly N–S) trending σ_1. The comparison between the obtained data and analog models of structural systems formed under variable loading conditions indicates that the observed features and the inferred stress fields in the Dead Sea rift are typical to oblique extension settings.

Keywords: Dead Sea rift; Fracturing; Faults; Stress fields; Fractal analysis; Earthquakes

1. Introduction

The Dead Sea rift extends for 1000 km from the northern Red Sea, to the south, to the East Anatolian Fault, to the north (Fig. 1). It consists of a series of basins bounded by steep-dipping faults with morphologically marked margins. The major basins in the south are the Gulf of Elat (Aqaba), the Dead Sea, the Lake Kinneret (Sea of Galilee) and the Hula Basin (Fig. 1). To the north of the Lebanese fault system are the basins of el-Gharb and Kara-Su. The basins are separated by threshold zones (inter-basin links) where the fault pattern is not evident in the morphology. Examples of the morphotectonic structures occurring within the investigated area are shown in Fig. 2.

* Corresponding author. Fax: +7 3952 426900.
E-mail address: lounina@crust.irk.ru (O.V. Lunina).

0264-3707/$ – see front matter © 2005 Elsevier Ltd. All rights reserved.
doi:10.1016/j.jog.2005.07.010

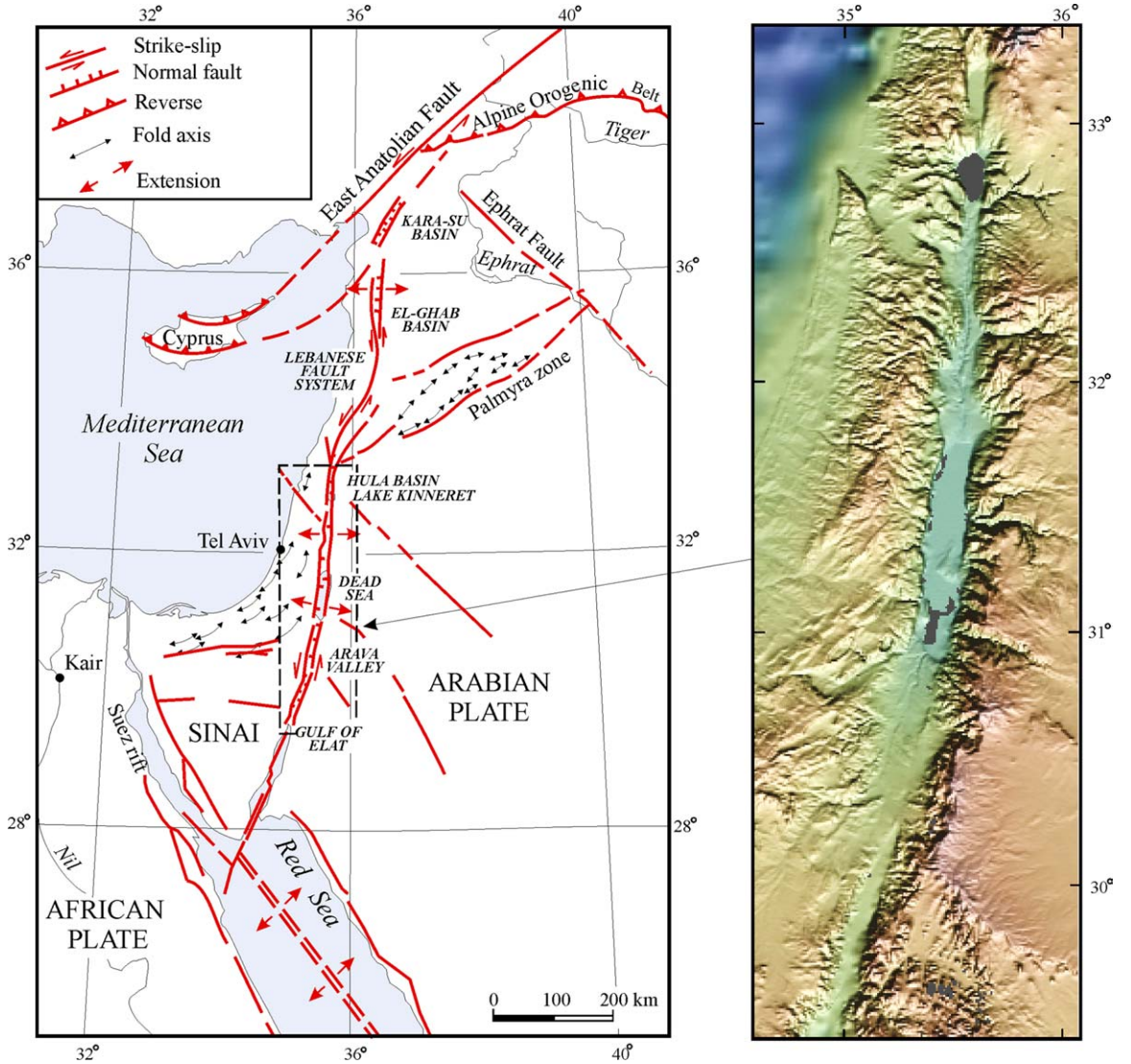

Fig. 1. Left: the tectonic framework of the Dead Sea rift and adjacent areas (after Darkal et al., 1990). The rectangle shows the investigated area. Right: digital shaded-relief map (from http://www.geomapapp.org).

The Dead Sea rift and the adjacent areas were the subject of many mapping campaigns, structural studies and the analyses of earthquakes focal mechanisms (Freund et al., 1970; Garfunkel, 1981; Kashai and Croker, 1987; Picard, 1987; Darkal et al., 1990; Van Eck and Hofstetter, 1990; Mart, 1994; Sneh, 1996; Shapira, 1997; Sagy and Reches, 2000; Horowitz, 2001; Mart et al., 2005 among others). Some of them were specifically dedicated to reconstruct the stress fields (Letouzey and Tremolieres, 1980; Eyal, 1996). Nevertheless, the development and geodynamics of the rift are a topic of intense discussion. The origin of the Dead Sea rift and its N–S orientation was attributed to: (1) E–W tension (Mart and Horowitz, 1981; Sagy and Reches, 2000; Horowitz, 2001); (2) NE–SW tension (Garfunkel, 1981); (3) N–S compression (Letouzey and Tremolieres, 1980) and (4) NNW–SSE compression and ENE–WSW tension (Eyal, 1996). The considerable variability of the local stress field is typical of the Dead Sea rift, which, like other fault patterns characterized by concurrent strike-slip and extensional tectonics, can lead researchers to different interpretations. In particular, according to Freund et al. (1970) and Garfunkel (1981), the Dead Sea rift is a transform fault, connecting the Red Sea oceanic spreading center with the East Anatolian Fault. Horowitz (2001) states that it is a “pure” rift, while Mart (1994) and Mart and Rabinowitz (1986) suggest that the Dead Sea rift is under the effects of both normal and left-lateral strike-slip displacements resulting from oblique extension. Tens of the contradictory

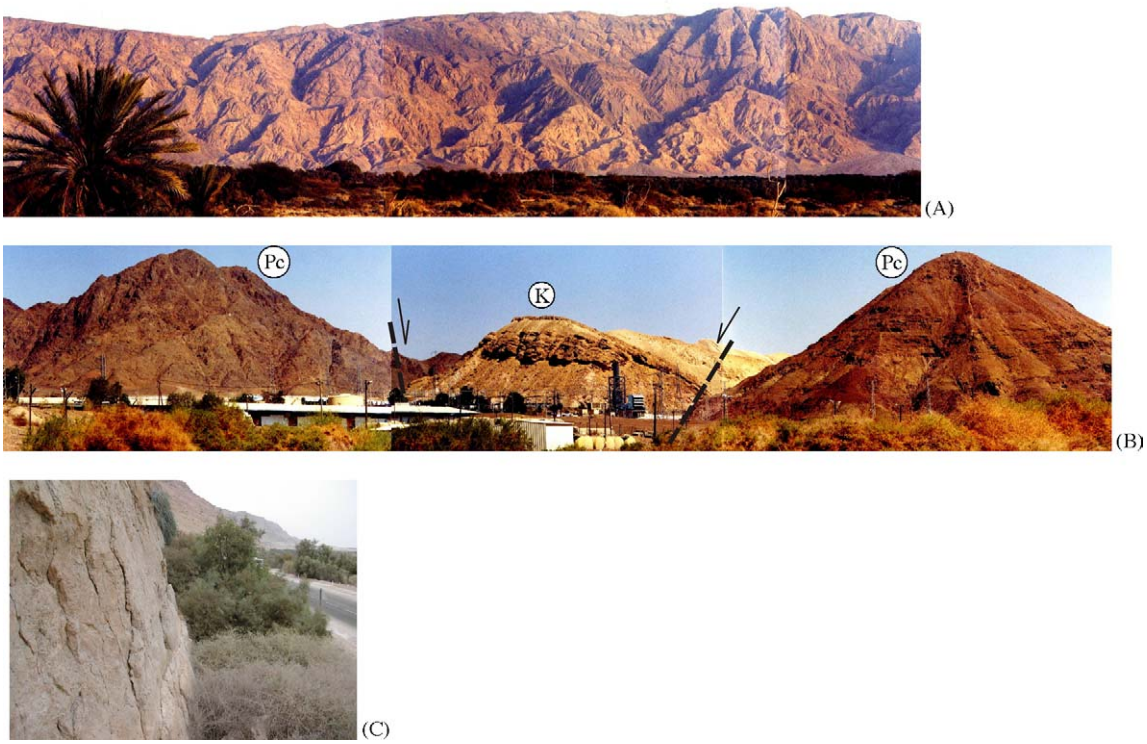

Fig. 2. Examples of morphotectonic structures occurring within the Dead Sea rift: (A) view to the eastern side in the southern part of the rift; (B) graben in the range of the western side of the rift, Southern Israel (Cretaceous limestone is in the central part, Precambrian basement is to the right and left); (C) steep fault plane in the western side of the rift.

arguments giving evidences for the benefit of that or another hypothesis of the development of the Dead Sea rift have been published; however, the peculiarities of the fault structure have received little attention. Furthermore, it is well known that any fault system of whatever genesis has an appropriate inner structure that reflects the corresponding conditions of its formation. Some historical information about faults of the investigated area is given below.

The fault distribution of the rift and its adjacent areas is the product of several faulting phases that differ in age and orientation. According to Horowitz (2001), the NW–SE trending normal faults and E–W trending strike-slip faults occurred during the Eritrean phase during Late Miocene and Pliocene. Insignificant uplift and abundant volcanism is typical of this event. Other studies (e.g., Mart and Horowitz, 1981) show that the Eritrean phase mainly generated the system of E–W trending dextral strike-slip faults and two systems of secondary faults trending NW–SE and NE–SW. The Levantine phase, which had been active since the Pliocene-Pleistocene, formed the Dead Sea rift and its uplifted shoulders. At this time, the E–W dextral strike-slips could compensate the extension along the rift (Horowitz, 2001). Kashai and Croker (1987) considered that a set of structural characteristics of the rift phase comprises the NW–SE and NE–SW crescentic faults that occur in three opposing pairs along the Dead Sea, Lake Kinneret and Hula basins. It should be noted that the fault pattern on the various geological maps (Picard et al., 1965; Sneh et al., 1998 and others) is noticeably inconsistent. In the present study, one of the last-published maps (Horowitz, 2001) compiled from several sources is used, though it does not include the whole rift (Fig. 3).

Thus, the significance of the faults in the rift structure is ambiguous. This ambiguity is one of the reasons of the vague understanding of its tectonic origin. The main purpose of the present study is to illuminate the peculiarities of the development of the fracturing patterns, the most indicative of the different stress fields occurring in the Dead Sea rift and suggest the prevalence of the Late Cenozoic principal stress directions. Meso-structural and statistical analysis methods (Gzovsky, 1975; Price and Cosgrove, 1990; Nikolaev, 1992; Hancock, 1991; Twiss and Moores, 1992) were used to infer the major fracturing patterns and the state of stress controlling the evolution and the geodynamics of the region.

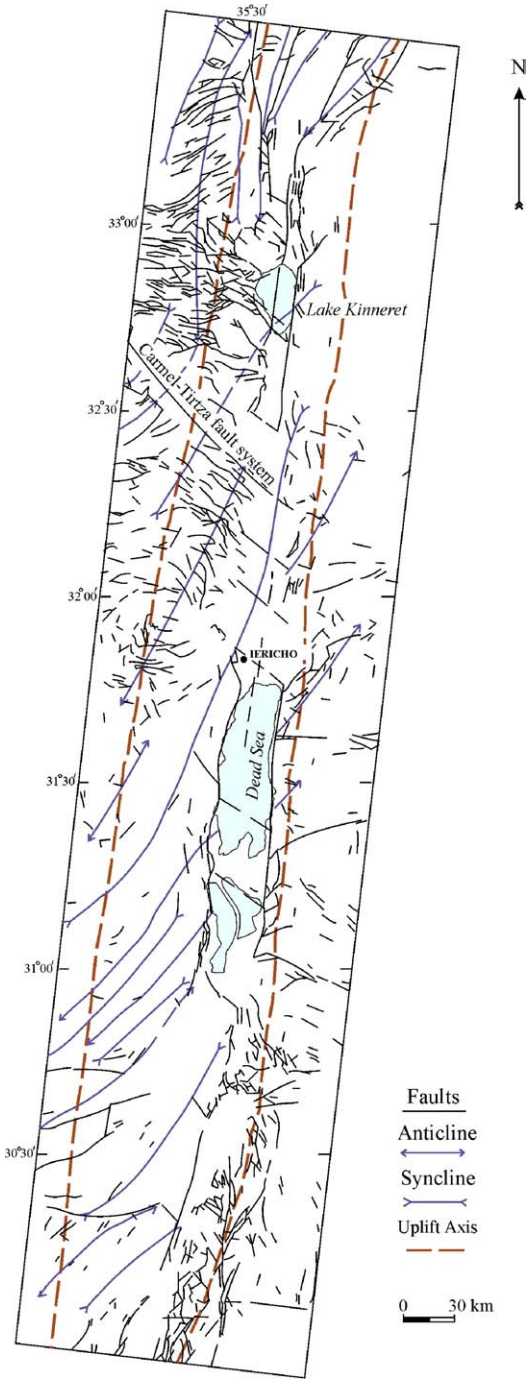

Fig. 3. Structural map of the Dead Sea rift (redrawn from Horowitz, 2001).

Seismicity is another reflection of the prevailing faulting and tectonic activity. Strong earthquakes that produced ground deformations occurred in the past 4000 years along Dead Sea rift (Amiran, 1951; Turcotte and Arieh, 1988; Shapira, 1997; Galli and Galadini, 2001). However, instrumental seismic records along the investigated area show comparatively low seismic activity that may suggest that the faults are currently locked (Zilberman et al., 2000). Therefore, the fractal analysis of the epicentral field of earthquakes of the Dead Sea rift and adjacent areas in the Southeastern Mediterranean over the period of 1983–2002 was carried out to characterize the specific role of different

segments of the fault structure. We consider the epicentral field as a totality of the earthquake epicenters on a territory for a certain time period. Below in the text, we use the term “epicenter area” for a single historical seismic event.

2. Structural study and data analysis

2.1. Initial data

The present structural research was carried out within the Dead Sea rift from the Gulf of Elat to the Hula basin based on 20 observation sites (Fig. 4). The detail description of the outcrops and measurements of the spatial (azimuth of dip and angle of dip), kinematic (slickensides and displacement of markers) and quantitative parameters of the fractures and fault zones (length of fractures and width of fault zones) that have not been healed were made during our field investigations. Extension and shear fractures were separated directly during the field-work. We have paid a special attention to the study of zones where the rock was intensively crushed and fractured and have characterized structural relationships between the fracture systems. The measurements of the shear fractures were also used for the construction of stereonets (Fig. 4), data analysis and stress field reconstruction in 16 of the measurement stations. As a whole, more than 1600 measurements of the fractures were obtained, of which 35 associated with slickensides and displacements.

We present the results of the study of fracturing and fault zones measured in the crystalline and sedimentary rocks, the age of which ranges from Precambrian to Pleistocene. It provokes the most challenging problem of assessing ages of the tectonic deformations and stress fields reconstructed from them. However, the occurrence of the fracture systems of the same orientation in the old and Late Cenozoic rocks (Fig. 4) likely suggests that the measured fractures formed or were reactivated at least during the Levantine phase (since the Pliocene-Pleistocene). The previous data obtained from tectonic fractures in various stratigraphic complexes at the Dead Sea rift and other seismically active regions are also well correlated due to imposed deformations associated with movements along active faults (e.g. Mart and Horowitz, 1981; Pavlides and Mountrakis, 1987; Sherman and Dneprovsky, 1989). Moreover, our observation sites are located within epicenter areas of the last historical destructive earthquakes that were accompanied by faulting of archaeological sites (Table 1). Based on the work of Marco et al. (2003), we constrained the minimal area of possible seismic offset for the each earthquake including the epicenter and the destroyed archaeological site (Fig. 4).

2.2. Orientation and significance of fracturing patterns

The maxima on the diagrams of the orientation measurements (Fig. 4) indicate that the N–S rift trend of the fractures is the principal one (or equal to others) at nine observation sites (GE2, AV1 and AV2—in the southern segment; DS1 and DS2—in the central segment; LK2, LK4, HB2 and HB3—northern sector of the investigated area). In general, N–S direction dominates the fracture systems in the Dead Sea rift (Fig. 5A). N–S trending systems are mainly steeply dipping (70–80°) and have the traces of the sub-vertical displacements in the form of the normal faults of the marker horizons (Fig. 6A), as well as dip-slip slickensides (Fig. 6B). Strike-slip offset was recorded only in site HB2 at the walls of the crusader castle of Vadum Jacob (Ateret) disposed just southern the Hula basin (epicenter area I in Fig. 4). The largest displacement measured along a single fracture is 0.5 m (Fig. 7A). The earlier mentioned value of 2.1 m sinistral offset (Zilberman et al., 2000) is probably the cumulative value measured along several fault segments. Indeed Marco et al. (1997) and Ellenblum et al. (1998) suggest that 2 m offset of the castle represents the cumulative slip of two or three earthquakes (1202 AD, 1759 AD and/or 1837 AD). Concurrently, the most deformed wall of the crusader castle has traces of the oblique displacement (Fig. 7B). A zone of normal fault offset with the apparent thickness of 1.0–1.5 m and dip angle 60° to the east in the Pleistocene sandstone with some gravel is measured below the eastern walls of the castle, at the foot of one of the levels of the fault scarp (Fig. 7C). The existence of more than 20 m normal displacement, 15 m of which occurred in the last 4–5 ka, is established for the Azaz fault along the eastern side of the Hula basin (Zilberman et al., 2000), approximately 15 km to the northeast from the crusader castle of Vadum Jacob.

The evidences of opening fractures and normal displacements along N–S faults produced during the 749 AD (Marco et al., 2003) and the 363 AD seismic events (Galli and Galadini, 2001) were also found in other archaeological sites (Table 1, Fig. 4). The 0.5–1 m opening along a N10°W trending fracture in the western wall of the Roman-Nabatean reservoir of Qasir el Telah was associated with 0.5–1 m sinistral strike-slip. The more the fault strike deviates from the N–S to NE the more the strike-slip component is evident. Thus, the strike-slip slickensides were measured along

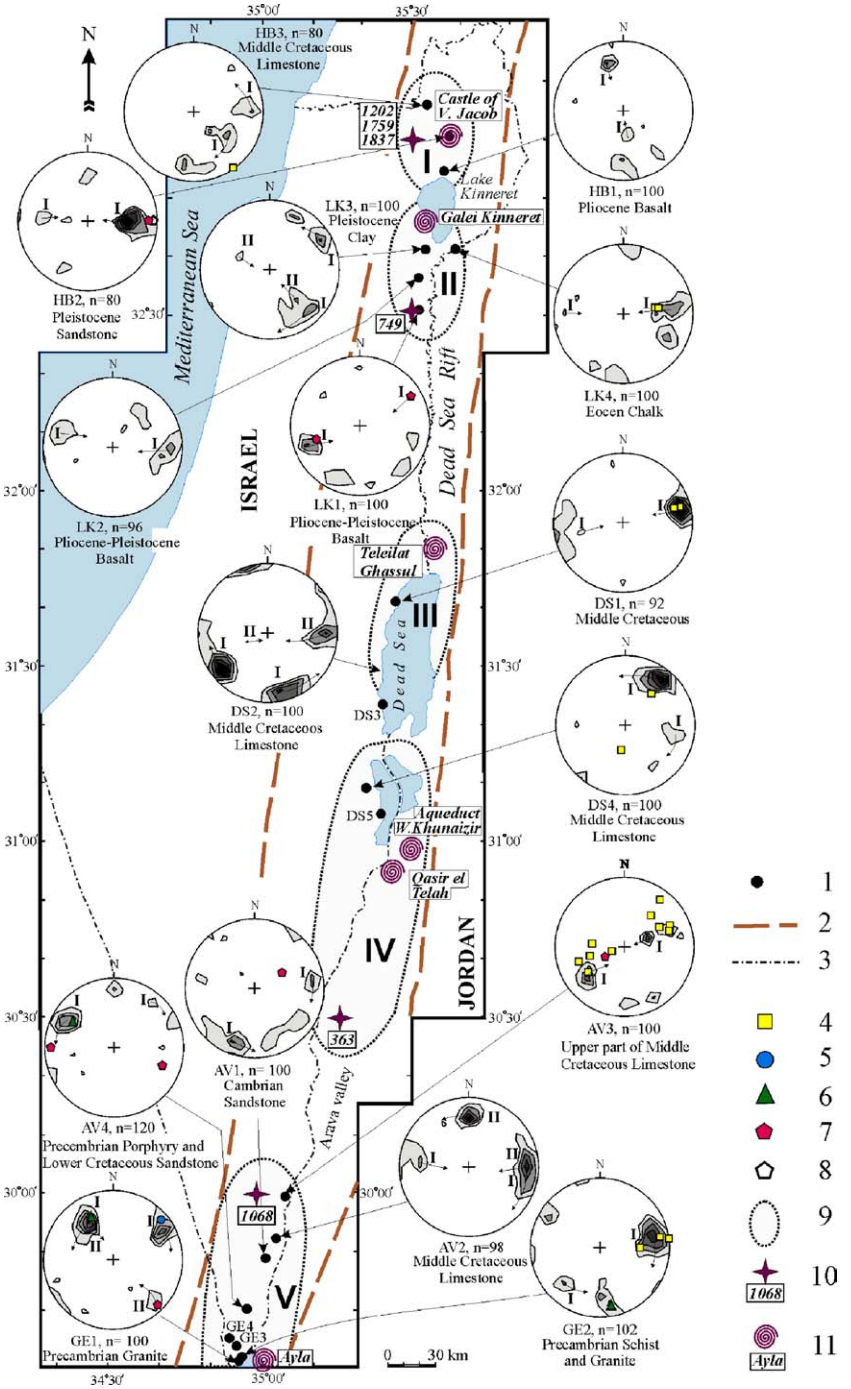

Fig. 4. Observation sites and fracturing diagrams (equal-area upper hemisphere projection). Intensity isolines are 3.5, 7.5, 9.5% and more; DS1: site label, *n*: number of measurements. Roman numerals and arrows on the diagrams show the pair of conjugate shear fracture systems. 1: observation site; 2: uplift axis of the rift; 3: international boundary; 4–8: fractures, on which there were found—4: dip-slip slickensides (60–90°); 5: oblique slickensides (30–60°); 6: strike-slip slickensides (0–30°); 7: normal fault displacements; 8: strike-slip displacements; 9: epicenter areas of the historical earthquakes (roman numerals indicate the areas according to Table 1); 10: proposed epicenter of the earthquake and date; 11: archaeological site faulted during the earthquake.

Table 1
List of destructive earthquakes associated with faulting of archaelogical sites in the Dead Sea rift (compiled from Galli and Galadini, 2001; Marco et al., 2003; Zilberman et al., 2000 and own observations)

Number of epicenter areas of the historical earthquakes according to Fig. 4	Date of earthquakes and possible magnitude (M)	Destroyed archaeological sites	Trend of the surface ruptures	Sense of slip and displacement	Adjacent sites of structural study
I	20 May, 1202 AD, $M \geq 7.5$; 25 November, 1759 AD, $M = 7.4$ and 1837 AD	Crusader castle of Vadum Jacob (Ateret)	N–S	Sinistral strike-slip, 0.5 m	HB1; HB2; HB3
			N–S	Opening, 0.28 m; sinistral strike-slip, 0.23 m; normal fault, 0.07 m	
			N–S	Sinistral strike-slip, 2.1 m (cumulative)	
II	18 January, 749 AD, $M \geq 7$–7.5	Galei Kinneret site in the city of Tiberias	354°	Normal fault, 0.35–0.5 m	LK1; LK2; LK3; LK4
			320°	Normal fault, 0.9–1 m	
			N–S	Normal fault, 0.1 m	
III	3600 BP	Telleilat Ghassul site	50°	Reverse, tens of centimeters	DS1; DS2; DS3;
			E–W	Undefined	
			NNW–SSE	Reverse	
			Undefined;	Normal fault, 0.5 m	
			NE–SW	Thrust	
IV					
	363 AD, $M \geq 6.5$	Water reservoir of Qasir el Telah	10°	Opening, 0.5–1 m; sinistral strike-slip, 0.5–1 m (real), 1.5–2 m (proposed)	DS4; DS5
		Aqueduct Wadi Khunaizir	20°	Dextral strike-slip, 2 m	
			N–S	Normal fault, few decimeters	
V	1068 AD	Ancient Ayla (the present Aqaba)	NE–SW	Sinistral strike-slip	GE1, GE2; GE3; GE4; AV4; AV1; AV2; AV3
			NNE–SSW	Mainly sinistral strike-slip	

NNE–SSW and NE–SW trending fractures in sites GE1 and AV4 (Fig. 4) within the epicenter area of the 1068 AD earthquake, 20–30 km far from the site wherein the walls of the ancient Ayla are shifted sinistrally (Table 1, epicenter area V in Fig. 4) (Galli and Galadini, 2001).

The N–S fracturing systems clearly manifest themselves mainly within the basins where the rift is well developed, with an exception of sites GE1, AV4, AV3 and DS4 (Fig. 4) where other fracture systems prevail on the N–S orientation. Two sites (GE1 and AV3) occur in the NE–SW and NW–SE trending fault zones, respectively. On the other hand, the intensity maxima of the fracturing corresponding to the rift direction were not observed at the three of four sites (LK1, LK3 and HB1) that are located within the elevated threshold zones, south and north of Lake Kinneret.

The data show that E–W, NE–SW and NW–SE fracturing systems are of rare occurrence (Fig. 5A). The E–W (270–280°) and NW–SE (310–320° and 340–350°) orientations among them are the most widespread and the NE–SW (40–50°) orientation has the least occurrence. Some kinematic indicators document normal (sites AV3, AV1, DS4 and LK1) and oblique (site GE1) displacements along the NW–SE fractures; strike-slip offsets (site GE2) – along the E–W fractures; strike-slip (sites GE1 and AV4) and normal (sites GE1 and HB3) – along the NE–SW fractures (Fig. 4). The occurrence of similar displacements in the archaeological relics and historical sedimentary sequences (Table 1) confirms that such slips are characteristic of the Late Cenozoic. A normal offset of 0.9–1 m was found along a fault

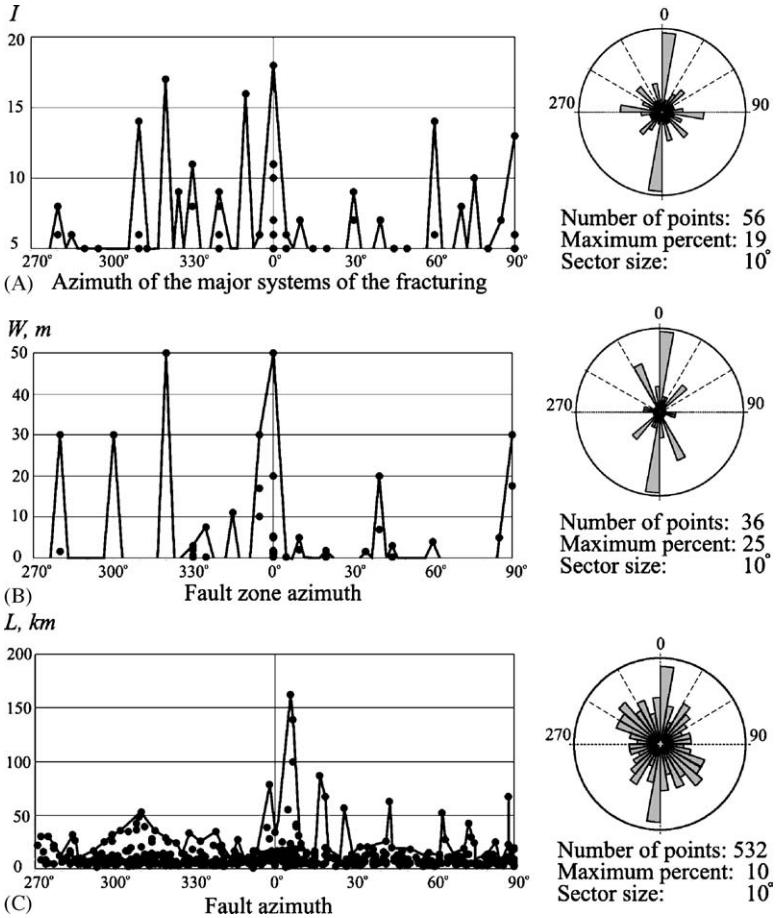

Fig. 5. Statistical analysis of structural data from the Dead Sea rift: (A) the intensity (I) of the major fracture systems with $I > 5$ (from stereonets, see Fig. 4) vs. their azimuth and corresponding rose-diagram; (B) width (W) of crushed and fractured zones along faults with $W > 0.1$ m vs. fault azimuths measured at the different sites and corresponding rose-diagram; (C) fault length (L) vs. fault azimuth measured within uplift axes of the rift (from the structural map, see Fig. 3) and corresponding rose-diagram.

plane trending 320° at the Galei Kinneret site (Table 1, epicenter area II in Fig. 4) in the city of Tiberias (Marco et al., 2003). Kinematics of E–W trending fractures traced in calcolihic ash and camp floor deposits dated 3600 years BP is indefinite (Galli and Galadini, 2001). However, occurrence of the E–W fractures in such young layers is an evidence of their activity in the Levantine phase. We have already mentioned the finds of sinistral strike-slip along the NNE–SSW and NE–SW trending faults in the walls of the ancient Ayla. Notably, some NE–SW fractures have traces of other senses of slips. Such cases were observed in the aqueduct of Wadi Khunaizir wherein the 2 m dextral strike-slip occurred during the 363 AD earthquake. The reverse faults and thrusts along NE–SW and NNW–SSE fractures formed during 3600 years BP earthquake in the Telleilat Ghassul site (Galli and Galadini, 2001). The different sense of slip along the faults of the same strike and age can be explained by short-term variations of stress fields (Caputo, 2005). Similar variations are known from the focal mechanisms of the recent seismic events (e.g. Van Eck and Hofstetter, 1990; Shapira, 1997).

To estimate the significance of the prevailing fracturing systems, we made a graph of the distribution of their azimuth versus their maximum intensity (I) (Fig. 5A). The graph clearly shows that the greatest intensity is characteristic to the fracturing systems trending N–S and NW–SE. The plotted I-values of the fracturing maxima tend to increase in the southern (west margin of the Elat Gulf and Arava valley) and central parts of the investigated area (Dead Sea basin) as compared with the northern part (Lake Kinneret and Hula basins and adjacent inter-basin links). The HB2 site is the only exception (Fig. 4).

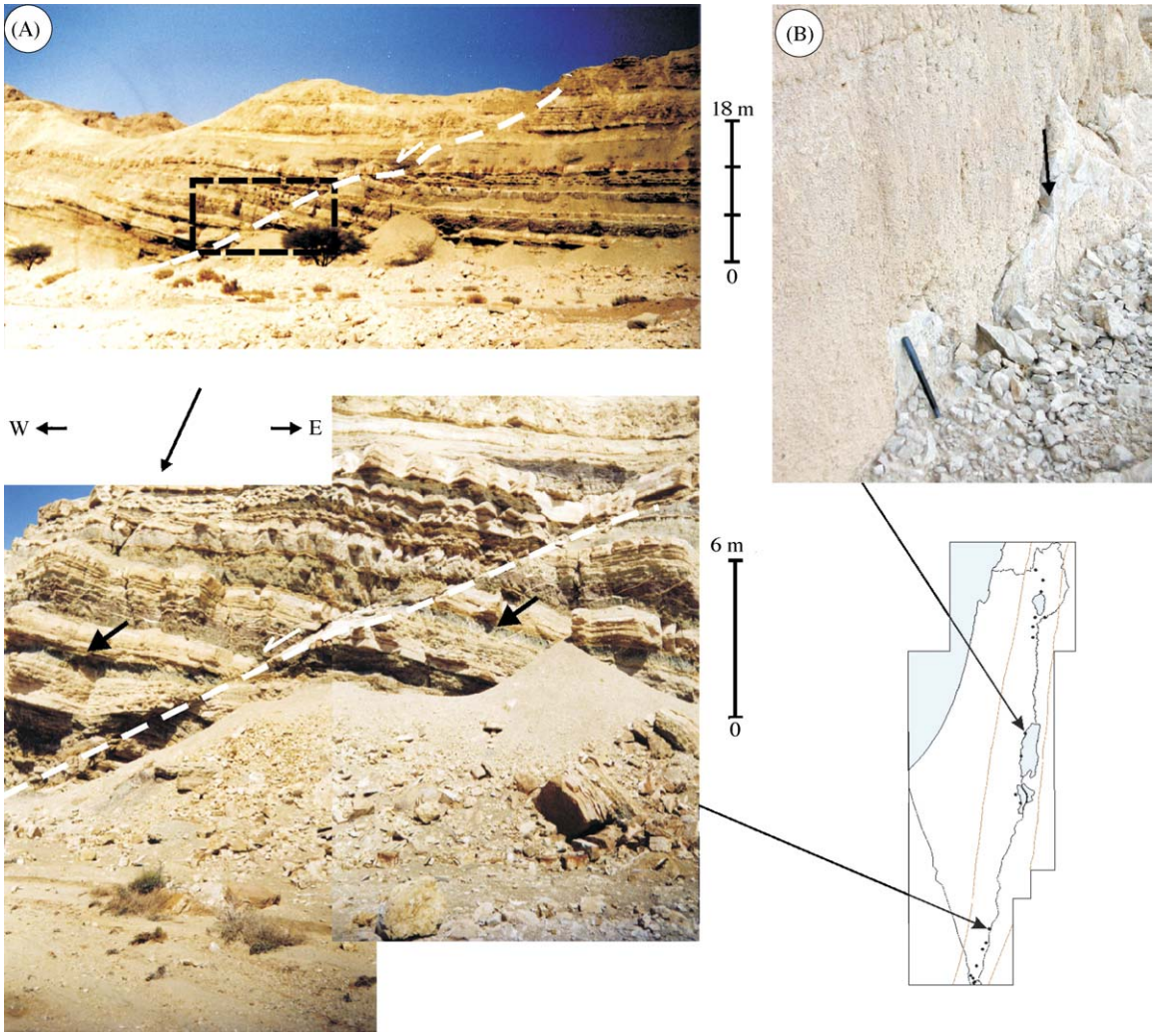

Fig. 6. Traces of the sub-vertical displacements along the near N–S fractures: (A) Normal fault displacement (dip azimuth of the fault is 240–270°, dip angle is 30–40°, displacement is 6–8 m, western side of the Arava valley, site AV3); (B) dip-slip slickensides (dip azimuth of the fracture is 75°, dip angle is 75–80°, western side of the Dead Sea basin, site DS1).

A similar statistical analysis was carried out for fault zones, where the spatial characteristics and width (*W*) of the zones of rock crushing and fracturing were measured. The rose diagram (Fig. 5B) shows that the most abundant group is oriented N–S (0–10°) and the second one, NW–SE (330–340°). The faults trending NE–SW (40–50°) occur less frequently and the E–W trending faults do not have any considerable occurrence against the background of the rest of the faults.

A similar analysis was also carried out for azimuths and length (*L*) of the faults (Fig. 5C). These parameters were measured from structural maps (Fig. 3) and only those faults that are located within the rift between the uplifted axes, or cross them, were included in the analysis. The main N–S orientation (0–10°) and the NW–SE (290–340°) orientation that forms quite diffused maximum are evident in the rose diagram (Fig. 5C). The NE–SW fault orientation is somewhat secondary and the E–W trend disappears completely within the rift valley.

Statistical analysis of the parameters of the faults and fractures shows that the structural pattern in the Southern Dead Sea rift mainly consists of a uniform set of the N–S trending faults (0–10°), the most widespread and significant and a more scattered set of secondary faults trending NW–SE, the azimuths of which vary from 290° to 340°. The NE–SW and E–W trending fault systems are subordinate to the two previous sets. The presence of the E–W maximum on the rose diagram for the fracturing (Fig. 5A) and its absence on the rose diagrams for the faults (Fig. 5B and C) suggests that the

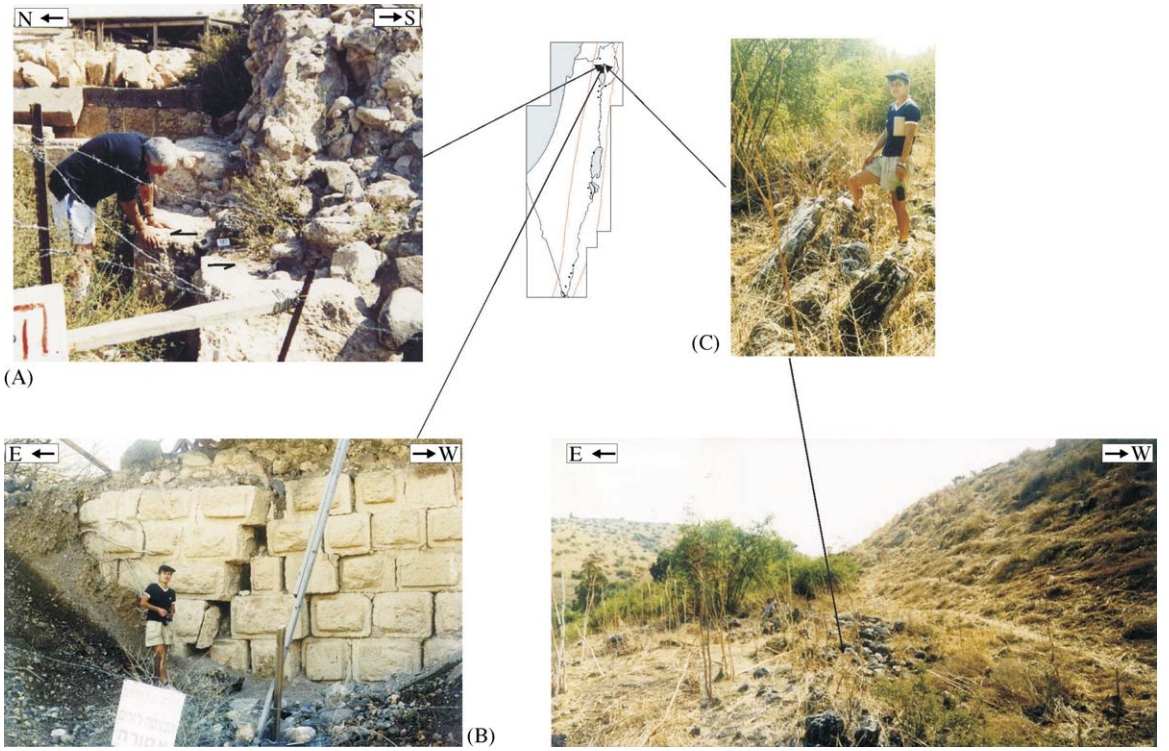

Fig. 7. Deformation of the walls in the crusader fortress of Vadum Jacob, south of the Hula basin, sequels of the 1202 and 1759 (?) earthquakes and the nearest outcrop (site HB2): (A) sinistral strike-slip, displacement is 0.5 m; (B) the deformed northern wall of the fortress with traces of oblique displacement. Opening is 0.28 m, sinistral strike-slip is 0.23 m, normal fault offset is 0.07 m; (C) morphology of the normal fault-scarp and location of the fault zone in the hanging block, about 5–10 m below walls of the crusader fortress of Vadum Jacob (after Marco et al., 1997; Ellenblum et al.,1998; Mart et al., 2005 with supplement).

former does not always reflect large fault structures. More often it indicates small fractures, the development of which did not lead to the occurrence of the E–W trending fault zone in most cases. Perhaps, other processes connected with rifting impeded an intensive development of the E–W fractures at the stage of tectonic evolution of the Dead Sea rift.

3. Stress fields

3.1. Methods of identification of conjugate shear fracture sets and reconstruction of principal stress axis directions

The relationship between fractures and principal stress directions implied by the Coulomb fracture criterion suggests that we can use fractures to estimate the directions of the principal stresses (Price and Cosgrove, 1990; Hancock, 1991; Twiss and Moores, 1992). As this takes place, it is essential to reliably identify the conjugate shear fracture sets that formed or were reactivated at the same time.

We separate the conjugate shear fracture systems from other set of fractures in two stages. First, the conjugate fracture sets are determined by using criteria such as confluence of the fractures, their mutual intersection, opposite sense of displacement, constancy of the angle between them under a general change of their orientation, analogous distribution and connection with regional structures (Gzovsky, 1975; Twiss and Moores, 1992). Second, the statistical analysis of the fracture diagrams is carried out using Nikolaev's (1992) method. The latter is almost unknown in the international literature but is widely applied in Russia. Therefore, we summarize the main points from the above reference.

The used method is primarily based on the fundamentals of rock mechanics, which suggest that two possible orientations of conjugate shear fractures can develop under the influence of homogeneous stress field. Nikolaev (1992)

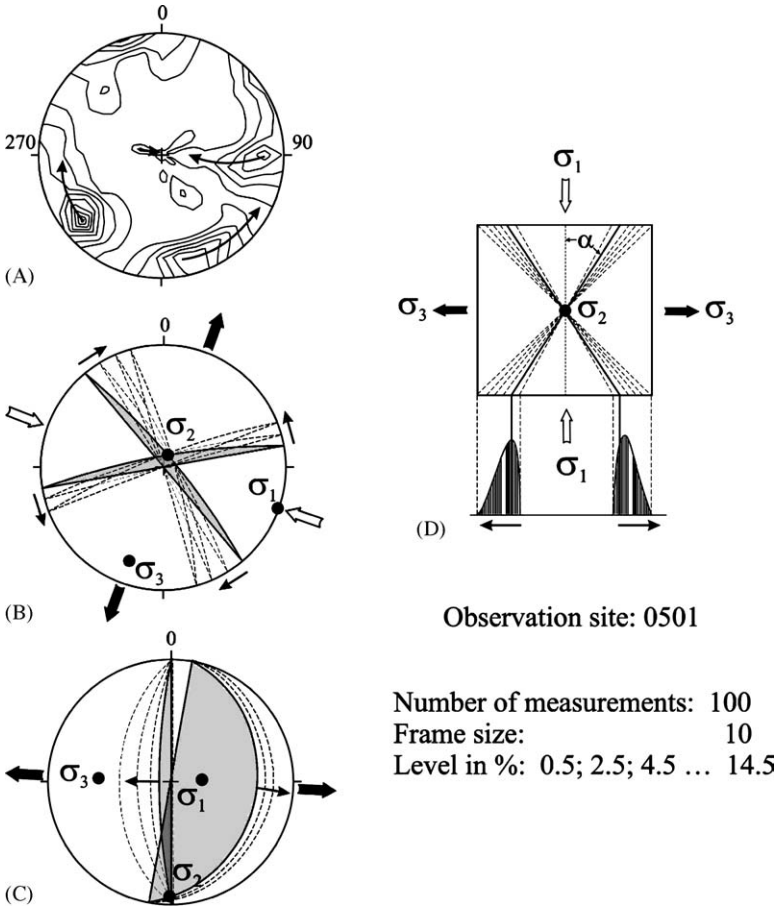

Fig. 8. Example of statistical analysis for the determination of the conjugate fracture systems and reconstruction of the principal stress directions (equal-area upper hemisphere projection): (A) fracturing diagram, arrows show the scattering directions within maxima, thus indicating the conjugate systems by Nikolaev's method (1992); (B, C) diagrams of the principal stress directions (σ_1, σ_2 and σ_3 are the compressional, intermediate and tensional stress axes, respectively); (D) scheme of the scattering development, α, angle of shear.

proved that the development of shear fractures is often associated with the formation of regular scattering in their orientation. The scattering of the conjugate shear fracture systems is opposite to each other (Fig. 8A and D). Its direction is connected with the principal stress axes and it is not influenced by heterogeneities. It should be noted that extension fractures do not form regular scattering. Mechanism of formation of the directional scattering in the orientation of the shear fractures is explained by complex effect. The propagation of each new fracture causes the redistribution of stress values and therefore changes the constraints, in which the subsequent fractures develop. During the development of the conjugate shear fractures, the angle of shear varies as a function of the confining pressure and the general decrease of stresses in the deformed rock volume. Therefore, the resulting scattering in orientation of the shear fractures is directed from compressional axis to tensional axis. According to the Nikolaev's (1992) method, three conditions should be fulfilled to separate the conjugate shear fracture systems from other fracture sets: (1) the maxima on the fracturing diagram must possess the prominent opposite scattering (Fig. 8A) derived from the tectonic stress field (Fig. 8B, C and D); (2) the maxima must lie on a great circle of projection; (3) the angle between the conjugate maxima must be not less than 30°. Only those fracture sets with the conjugation confirmed by the statistical criteria are used for the reconstruction of the principal stress directions.

Following the identification of shear fracture systems the principal stress axes can be inferred based on: (1) the line of intersection of the conjugate faults is the intermediate stress axis (σ_2); (2) the compressional stress axis (σ_1) bisects the acute angle between the fault planes and (3) the tensional stress axis (σ_3) bisects the obtuse angle (Gzovsky, 1975; Price and Cosgrove, 1990; Hancock, 1991; Twiss and Moores, 1992) (Fig. 8B, C and D).

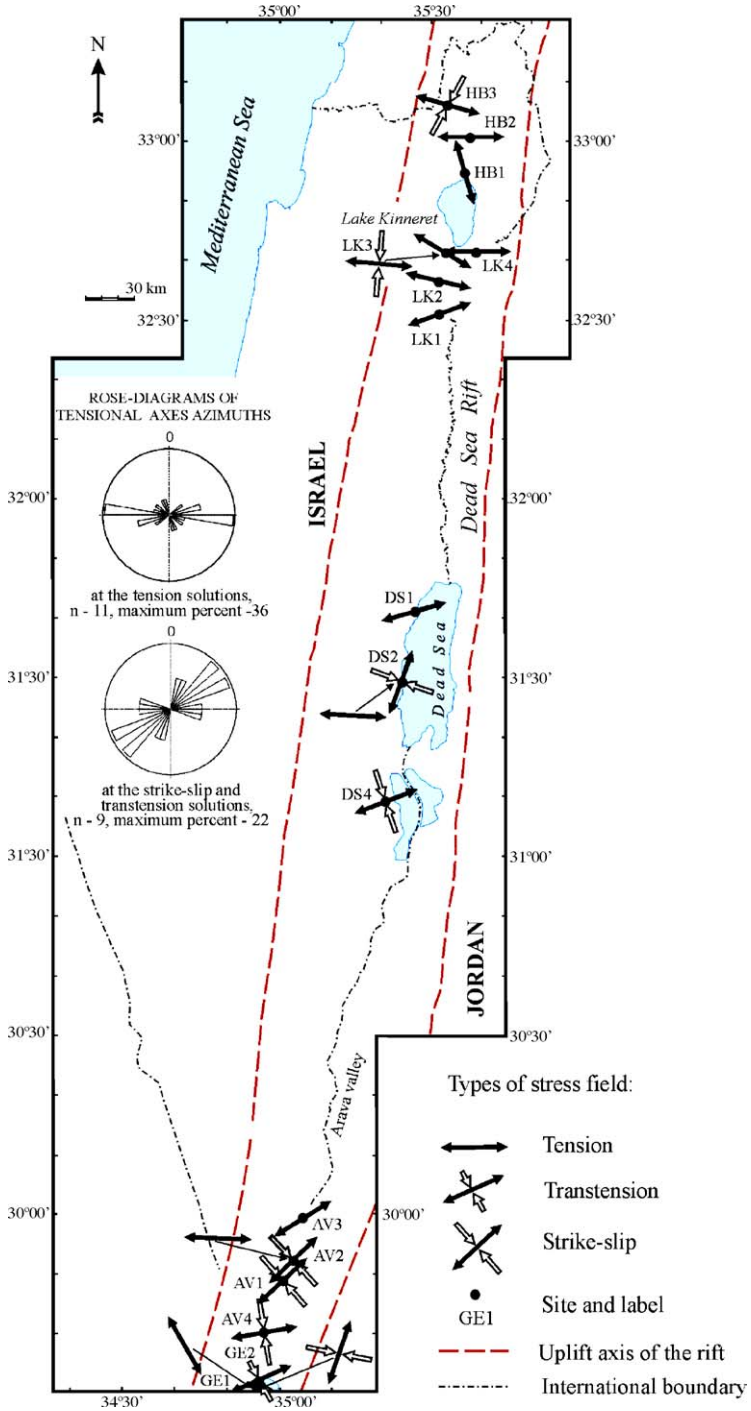

Fig. 9. Stress fields of the Dead Sea rift from fracturing data.

3.2. Results of the reconstructions of the stress field

The results of the structural reconstructions (Fig. 9) along the Dead Sea rift show three types of stress fields. They are grouped by spatial orientations of the principal stress axes with regard to horizontal:

Tension	σ_1 = 61–90°	σ_2 = 0–30°	σ_3 = 0–30°
Transtension	σ_1 = 31–60°	σ_2 = 31–60°	σ_3 = 0–30°
Transcurrent	σ_1 = 0–30°	σ_2 = 61–90°	σ_3 = 0–30°

where the σ_1, σ_2 and σ_3 are the compressional, intermediate and tensional stress axes, respectively.

Two different solutions were obtained at four of the 16 sites (GE1, AV2, DS2 and LK3). One solution is associated to a pure tensile regime, the other to strike-slip deformation. As a whole, the most widely diffuse type of stress field is tension obtained from 11 sites where σ_3 has a general E–W orientation or slightly deviated anticlockwise. This stress field occurs in rocks of different ages and is best manifested in the northern sector of the investigated area, affecting Plio-Pleistocene basalts and Pleistocene sedimentary deposits. In sites GE1 and HB1, σ_3 is oriented NW–SE and probably reflects local variations of the stress state or an event that occurred before the Pleistocene.

The second group of stress solutions has been inferred in eight sites characterized by a transcurrent regime and in one site by a transtensile stress. In this group, a more scattered pattern of the principal stress directions is observed. In three sites occurring in Precambrian, Cretaceous and Pleistocene rocks (sites AV4, HB3 and LK3), the tensile axis has a nearly E–W orientation (80–110°). In four of them (sites GE2, AV1, AV2 and DS4), σ_3 is directed to NE–SW (40–50° and 60–70°) and in two of them (sites GE1 and DS2), σ_3 is directed to NNE–SSW (10–30°).

If we consider the ages of the sampled sites, only the E–W tensile stress field can be considered to be still active. This regime has been associated to the Dead Sea rift by different authors (Mart and Horowitz, 1981; Sagy and Reches, 2000; Horowitz, 2001). However, we cannot exclude that the other inferred stress fields recur as well, because focal mechanisms of numerous earthquakes show both strike-slip and normal faulting (Van Eck and Hofstetter, 1990; Shapira, 1997), suggesting that a complex stress field is still active.

It should be noted that more often fluctuations of the state of stress are observed in the southern sector of the rift than in the northern sector where the stress field is relatively stable in the principal stress directions. This can reflect peculiarities of the earth crust structure in the different parts of the rift; in particular it is possible that greater lithological heterogeneities occur in the segment of the Gulf of Elat–Dead Sea basin.

As a whole, the results of the stress field reconstructions show that two main types of local stress tensors are associated with the structural development of the Dead Sea rift: (1) pure tension with E–W (mainly) and ENE–WSW trending σ_3 and (2) transcurrent regime with NE–SW (sometimes near E–W) trending σ_3 and NW–SW (sometimes near N–S) trending σ_1.

4. Fractal analysis of the spatio-temporal variations of the earthquake epicentral field over the period of 1983–2002

4.1. Methods of evaluation of fractal dimensions

The approach that allows characterizing some features of the complex fractal sets (of seismicity) without resort to multi-fractal analysis was therewith used for the analysis of spatio-temporal variations of the earthquake epicentral field in the Dead Sea rift. A similar approach was previously applied for the Baikal rift zone (Sherman and Gladkov, 1999; Gladkov and Shishkina, 2002).

The catalogue of earthquakes recorded by the Israel seismic network (Fig. 10) and presented on the website of the Geophysical Institute of Israel – http://www.gii.co.il/html – was used in the process. The data include 7677 events with $M \geq 2.0$ registered over the period of 1983–2002 in the Southeastern Mediterranean (Fig. 10A, Table 2). Nine hundred and twenty two earthquakes from them occurred in the Southern Dead Sea rift for the same time period (Fig. 10B, Table 2). We did not include the events recorded before 1983 in the fractal analysis of the seismicity for lack of statistics. Thus, only 383 earthquakes are known from the above-mentioned catalogue over the period of 1963–1982 for the whole Southeastern Mediterranean.

To describe a spatial structure of the epicentral field, we used a classic box-counting technique (Mandelbrot, 1982; Turcotte, 1989). In doing so the radius R of the focus of earthquake with magnitude M was determined under the formula of Riznichenko (1976) (for a spherical focal model)

$$\log R_{\mathrm{km}} = -1.671 + 0.422M$$

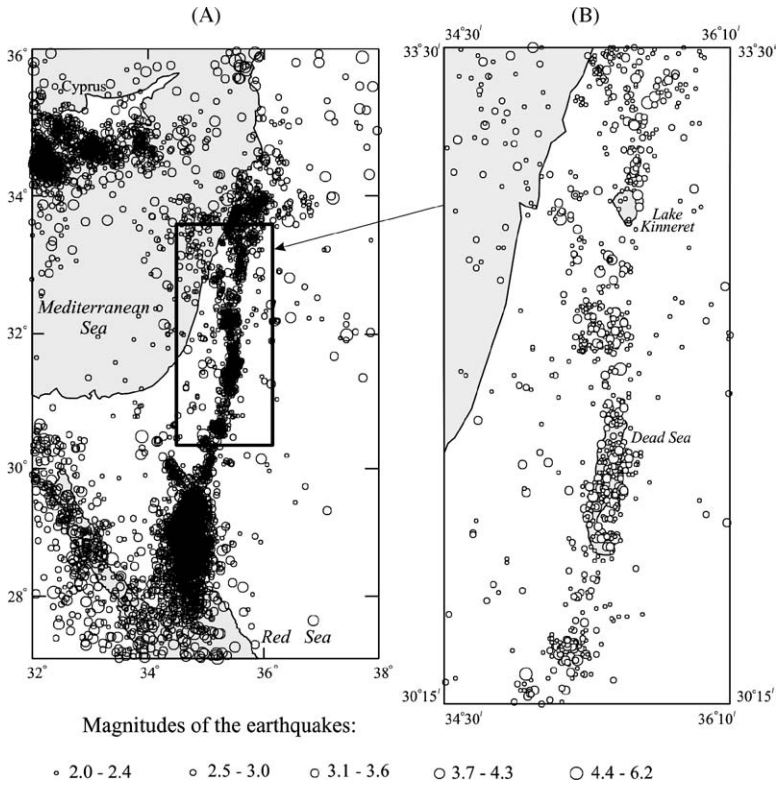

Fig. 10. Earthquake epicentral field (1983–2002): (A) in the Southeastern Mediterranean and (B) in the Dead Sea rift.

The value derived from the above formula allows to estimate a parameter of the earthquake focus as projected area of circle S on the surface

$$S = \pi R^2$$

On determination of fractal dimensions by the box-counting technique the S of all epicenters that fell within a single pixel of the corresponding dimension (L_0, L_1, …, L_i) were summarized at each stage of the iteration process and the pixel was considered to be destructed if the obtained value was more than 0.5% of its area. The data obtained in such a way allowed calculating fractal dimensions D_s as follows:

$$D_s = \frac{\log N_i}{\log L_i}$$

where N_i and L_i are the number of destructed pixels and the size of the system in the pixel's size units used for the ith iteration, respectively (Sherman and Gladkov, 1999).

Table 2
Results of the fractal analysis of the earthquake epicentral field over the period of 1983–2002

Time periods	Investigated areas			
	Southeastern Mediterranean (LON 32°00′–38°00′ LAT 27°00′–36°00′)		The Dead Sea rift (LON 34°30′–36°10′ LAT 30°15′–33°30′)	
	Number of events	D_s	Number of events	D_s
1983–1987	745	1.33 ± 0.03	260	1.56 ± 0.03
1988–1992	936	1.46 ± 0.02	305	1.56 ± 0.02
1993–1997	4946	1.56 ± 0.01	180	1.43 ± 0.02
1998–2002	1050	1.48 ± 0.04	177	1.48 ± 0.03

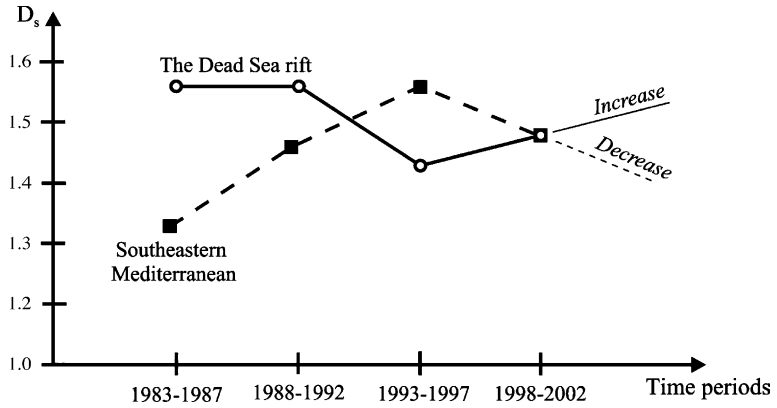

Fig. 11. Fractal dimensions of seismicity (D_s) vs. time.

Upon considering the spatial variations of the fractal dimensions, the investigated area within the Dead Sea rift was divided into 36 square sites. Fractals D_s were calculated for each of these sites from the above algorithm. The obtained D_s values were assigned to the center of each of these squares. If no fractal properties manifested themselves within any site (at the assigned boundary conditions), then the site was assigned a value of 0. The schemes in isolines were drawn from these data later on.

4.2. Results of the fractal analysis and their interpretation

Two data sets were analyzed. The first one included the seismic data on the Southeastern Mediterranean as a whole (Fig. 10A) and the second included the earthquakes that occurred in the Dead Sea rift (Fig. 10B). Each of these sets was broken up into four time periods: 1983–1987, 1988–1992, 1993–1997 and 1998–2002 (Table 2). The fractal dimensions typical to the general seismic destruction of the earth's crust were calculated for these periods. The obtained data show that the epicentral field in the Dead Sea rift is mostly opposite in phase to that in the Southeastern Mediterranean. It is evidenced by both the quantities of events and their fractal dimensions (Table 2, Fig. 11). When seismicity intensifies on the territory of the Southeastern Mediterranean as a whole, it decreases in the rift and so does the fractal dimension and vice versa. The seismic process is only synchronous on both investigated areas in the last 5-year period (1998–2002) as judged from the fractal dimensions. The mismatch between the decreasing number of seismic events and increasing fractal dimensions in 1998–2002 as compared to the previous time period (1993–1997) in the Dead Sea rift is indicative of larger energy release, on the average, per each earthquake in the latest period.

The analysis of the epicentral field in the Dead Sea rift shows that it is a complex fractal system consisting of a series of segments alternating increasing and decreasing fractal dimensions (Fig. 12). Most of the maxima are elongated and lined up emphasizing the general strike of the rift. At the same time, the maxima near the Dead Sea are somewhat shifted to the east of the axial zone of the rift, while in the vicinity of Lake Kinneret and to the north of it they are shifted to the west of it. The location of maxima changes little in different time periods, but their spatial dimensions and intensity vary rather considerably. Note that the location of the described maxima correlates well with the structural asymmetry of the rift. The eastern margin of the Dead Sea was uplifted by more than 4 km whereas the western margin was uplifted by only 2 km (Garfunkel, 1981; Mart and Horowitz, 1981). The asymmetry of the rift changes to the north of Lake Kinneret: the western flank becomes topographically and structurally higher than the eastern flank. It is probably related to the fact that the major seismocontrolling structures are traced just in these places along the rift basins. We also suppose that the northwestern turn of isolines of the maxima of fractal dimension values in 1988–1992 and 1998–2002 is due to the effect of the Carmel-Tirtza large fault system (Fig. 12).

The 5-year break (1993–1997) occurs when there is almost no fractality in the Dead Sea rift that results in the only weak maximum (Fig. 12). Perhaps it reflects the moment of structural reorganization directly in the rift. It coincides with a sharp growth of the earthquake number in the Southeastern Mediterranean as a whole (Table 2). Judging by the results of fractal analysis made from the four 5-year periods, an increase of seismic activity in the next 5 years can be expected in the Southern Dead Sea rift (Fig. 11).

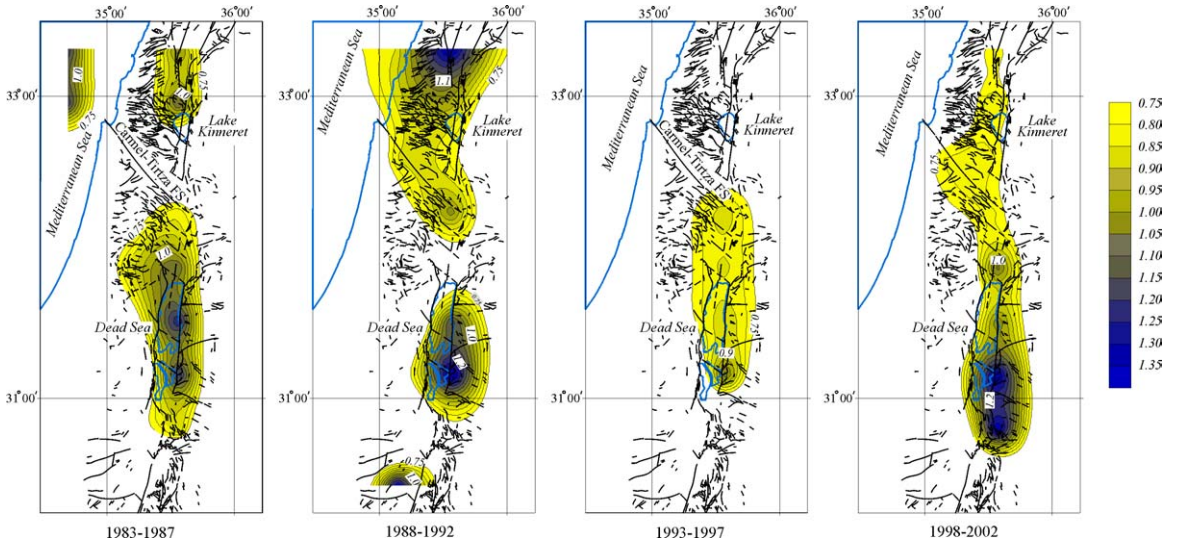

Fig. 12. Distribution of fractal dimensions D_s at different time periods in the Dead Sea rift.

5. Comparison of the obtained results with analogue experiments and discussion

Scaled analogue models have been successfully applied to the analysis of the deformation patterns resulting from strike-slip, pure and oblique extension (Withjack and Jamison, 1986; Tron and Brun, 1991; Brun and Tron, 1993; Dauteuil and Brun, 1993, 1996; McClay and White, 1995; Scott and Benes, 1996; Bonini et al., 1997; Mart and Dauteuil, 2000; Clifton et al., 2000; Corti et al., 2001 among others). Comparing our results with experimental results can shed some light on the condition of the structural development and geodynamic regime of the Dead Sea rift.

One of the obvious differences between oblique and orthogonal rifts, as well as strike-slip zones, is the range of fault azimuths (Withjack and Jamison, 1986; Bonini et al., 1997; Clifton et al., 2000). As experimental works show, when the α angle between the extensional vector and the rift axis is 90°, a large destructive zone presents one system of normal faults parallel to the direction of the developing rift (Clifton et al., 2000). The azimuth of faults varies steadily with decreasing α, reaching essential change, when $\alpha = 45°$ and 30°. A stable fault system in the models appears, the direction of which deviates up to 25–30° from the rift trend. Applied to the Dead Sea rift, the NW–SE trending maximum on the rose diagrams (Fig. 5) corresponds to that fault system. When $\alpha = 30°$ or less, a third fault system appears, which is perpendicular to the rift trend and plays a considerable role in the inner structure of the tectonic zone. It is more evident within the central model block (Clifton et al., 2000). As it has already been shown, the E–W oriented faults do not play a key role in the fault structure of the Dead Sea rift. The major and most extensive faults concentrate in the southern part of the rift and are independent fault structures that formed in the previous phase before an intensive development of the rift. This does not exclude their possible activity in the Levantine phase (since the Pliocene-Pleistocene), in which the E–W trending strike-slip faults could compensate for the extension (Horowitz, 2001). Thus, the comparison of the experimental data with the real structural setting suggests that the rift has undergone oblique extension, which led to the formation of two fault sets with N–S and NW–SE orientations, determining the architecture of the Dead Sea rift.

The comparison the historical destructive earthquakes associated with faulting of archaeological sites (Table 1) with our structural data shows that trends of the surface ruptures often repeat the orientations of the fracturing patterns measured in the crystalline rocks and sediments of different ages. Moreover, the fault kinematics observed in displaced archaeological relics coincides with that observed on parallel fractures on rocks. Table 1 obviously documents that the largest offsets are typical to the surface ruptures trending nearly N–S and NW–SE.

The fractal analysis helps understanding the spatio-temporal variations of the epicentral field in the Dead Sea rift and confirms that the present-day seismic activity is controlled by N–S and NW–SE trending structures. In Fig. 12 these two trends are emphasized by the maxima of fractal dimension confined to the structural zones traced along the

eastern coast of the Dead Sea (N–S trend), along the western board of Lake Kinneret basin and to the north of it (N–S trend) and along the Karmel-Tirtza fault system (NW–SE trend).

Clifton et al. (2000) show that in analogue modeling when $\alpha \geq 45^\circ$, the azimuth of very long faults coincides with the maxima of occurrence of faults of specific directions. This correlates with our data that reveal that the greatest intensity of the fracture systems, the largest width of the fault zone and, in many cases, their longest lengths coincide also with the maxima of azimuths on the rose diagrams (Fig. 5). When $\alpha = 30^\circ$ and 15°, these regularities break. Therefore, the regional extensional vector in the Dead Sea rift forms an angle ranging from 60° to 30° with respect to the rift axis. As a result, the regional stress field produces two main types of local stress tensors: the near E–W tensile regime and the transcurrent regime with NE–SW trending tension axis and NW–SE trending compressive axis (Fig. 9).

Based on the detailed statistical analysis of the directions of fractures and faults, we show the similarities between the fault patterns existing in the Dead Sea rift and those obtained by analogue models resulting from oblique extension. The inner structure, which is determined by en-echelon rift segments-basins separated by elevated threshold zones, is another typical feature of the oblique rifts (Picard, 1987; Mart and Dauteuil, 2000). This structure is emphasized by en-echelon faults with a displacement component varying from pure normal to strike-slip faulting (Corti et al., 2001). A strain partitioning between different sets of structures is observed in the experiments and fault dips are generally steeper than in pure normal faults (Tron and Brun, 1991). All these features are observed in the structural pattern and in the relief characterizing of the Dead Sea rift.

The 70–80° dip angles (usually typical of strike-slip faults) of many N–S faults and concurrently the structural evidences of the normal displacements along them can be also explained by the fact that considerable amounts of strike-slip movements could have occurred before the intensive rifting of the Levantine phase. At that time, the N–S faults could start developing with a transcurrent kinematics. Then extension became dominant and led to the formation of the Dead Sea rift, i.e. to the development of normal faults with non-characteristic angle dips. Similar changes of the stress state from transcurrent to tensile regime are documented in the Baikal, Barguzin and Kichera basins of the Baikal rift zone (San'kov et al., 1997). Taking this into account, we agree with Sneh (1996) that a transcurrent regime (Late Oligocene–Early Miocene) preceded the rifting phase.

Overall, the present research shows that the structure of the Dead Sea rift corresponds to neither a typical strike-slip fault nor to "pure" rift and it is likely the result of oblique extension.

6. Conclusions

The pursued investigations gave the chance to obtain new data on the fracturing patterns and stress fields in the Dead Sea rift (on the Gulf of Elat–Hula basin segment). Several historical cases of the surface faulting on archaeological sites (Galli and Galadini, 2001; Marco et al., 2003) and the fractal analysis of the earthquake epicentral field over the period of 1983–2002 allow to document that the revealed peculiarities in the fault patterns and stress fields are typical of the Late Cenozoic and probably present-day tectonic regime. The complex data analysis gives grounds to distinguish a number of specific features that are typical to oblique extension settings:

1. In the southern part of the rift, the fault network is characterized by the N–S faults, the trend of which is relatively stable within 0–10° and NW–SE secondary faults with azimuths spanning from 290° to 340°. Fault systems with other trends are less common and of lesser importance.
2. The N–S and NW–SE trending faults are the most extensive ones, have the largest crushed zones and represent the longest fracture systems.
3. Most of the N–S trending faults are well pronounced within the basins and often minor to other fault trends in the inter-basin links.
4. Meso-structural features document normal fault displacements along the major N–S faults within the basins, while in the inter-basin links the displacement component may vary from normal to strike-slip faulting within the same fault zone. The NW–SE faults are characterized by composite normal fault and oblique types of displacements, the E–W faults by purely transcurrent displacements and the NE–SW faults by oblique displacements.
5. Two main types of the local stress fields are associated with the structural development of the Dead Sea rift: (1) tensile with E–W (mainly) and ENE–WSW trending σ_3 and (2) transcurrent with NE–SW (sometimes near E–W) trending σ_3 and NW–SE (sometimes near N–S) trending σ_1.

6. According to fractal analysis of the earthquake epicentral field, large N–S and NW–SE trending fault zones traced along the eastern coast of the Dead Sea, along the western sector of Lake Kinneret basin and to the north of it and along the Carmel-Tirtza fault system are the major seismocontrolling structures.

Based on the results of the present study and the review of historical destructive earthquakes, it is likely that future large earthquakes occurring in the Dead Sea rift will produce the strongest ground deformations along faults and fractures trending nearly N–S and NW–SE.

Acknowledgements

We are grateful to Prof. Spyros B. Pavlides and Prof. Riccardo Caputo who gave the comments that improved this paper much. We wish to thank an anonymous reviewer for his constructive criticisms, helped as well refining the work. The research was supported by Haifa University (Israel) and the Russian Foundation for Basic Research (grants 04-05-64348, 04-05-64148).

References

Amiran, D.H.K., 1951. A revised earthquake catalogue of Palestine. Israel Explor. J. 1, 223–246.

Bonini, M., Souriot, Th., Boccaletti, M., Brun, J.P., 1997. Successive orthogonal and oblique extension episodes in a rift zone: laboratory experiments with application to the Ethiopian rift. Tectonics 16, 347–362.

Brun, J.-P., Tron, V., 1993. Development of the North Viking Graben: inferences from laboratory modeling. Sediment. Geol. 86, 31–51.

Caputo, R., 2005. Stress variability and brittle tectonic structures. Earth-Sci. Rev. 70, 103–127.

Clifton, A.E., Schlische, R.W., Withjack, M.O., Ackermann, R.V., 2000. Influence of rift obliquity on fault-population systematics: results of experimental clay models. J. Struct. Geol. 22, 1491–1509.

Corti, G., Bonini, M., Innocenti, F., Manetti, P., Mulugeta, G., 2001. Centrifuge models simulating magma emplacement during oblique rifting. J. Geodyn. 31, 557–576.

Darkal, A.N., Krauss, M., Ruske, R., 1990. The Levant fault zone. An outline of its structure, evolution and regional relationship. Z. Geol. Wiss. Berlin 18, 549–562.

Dauteuil, O., Brun, J.P., 1993. Oblique rifting in a low spreading ridge. Nature 361, 145–148.

Dauteuil, O., Brun, J.P., 1996. Deformation partitioning in a slow spreading ridge undergoing oblique extension: Mohns Ridge. Norwegian Sea Tectonics 15, 870–884.

Ellenblum, R., Marco, S., Agnon, A., Rockwell, T.K., Boas, A., 1998. Crusader castle torn apart by earthquake at dawn, 20 May 1202. Geology 26, 303–306.

Eyal, Y., 1996. Stress field fluctuations along the Dead Sea rift since the middle Miocene. Tectonics 15, 157–170.

Freund, R., Garfunkel, Z., Zak, I., Goldberg, M., Weissbrod, T., Derin, B., 1970. The shear along the Dead Sea. Rift. R. Soc. London Phil. Trans. A 267, 107–130.

Galli, P., Galadini, F., 2001. Surface faulting of archaeological relics. A review of case histories from the Dead Sea to the Alps. Tectonophysics 335, 291–312.

Garfunkel, Z., 1981. Internal structure of the Dead Sea leaky transform (rift) in relation to plate kinematics. Tectonophysics 80, 81–108.

Gladkov, A.S., Shishkina, L.P., 2002. Fractal analysis of the epicentral field of earthquakes on the southern flank of the Baikal rift zone (BRZ). In: Abstracts of the Contributions 27th General Assembly of the European Geophysical Society, Nica, France, 4 (CD-disk, ISSN: 1029–7006).

Gzovsky, M.V., 1975. The First Principles of Tectonophysics. Nedra Press, Moscow (in Russian).

Hancock, P.L., 1991. Determining contemporary stress directions from neotectonic joint systems. In: Whitmarsh, R.B., Bott, M.H.P., Fairhead, J.D., Kusnir, N.J., (Eds.), Tectonic Stress in the Lithosphere. Phil. Trans. Royal. Soc. London A 337, 29–40.

Horowitz, A., with contributions by Flexer, A., Ginzburg, A., Ben-Avraham, Z., Garfunkel, Z., 2001. The Jordan rift valley. A.A. Balkema publishers, Tokyo.

Kashai, E.L., Croker, P.F., 1987. Structural geometry and evolution of the Dead Sea-Jordan rift system as dedused from new subsurface data. Tectonophysics 141, 33–60.

Letouzey, J., Tremolieres, P., 1980. Paleo-stress fields around Mediterranean derived from microtectonics: comparison with plate tectonic data. Rock Mechanics 9, 173–192.

Mandelbrot, B.B., 1982. The Fractal Geometry of Nature, New York.

Marco, S., Agnon, A., Ellenblum, R., Eidelman, A., Basson, U., Boas, A., 1997. Eight hundred and seventeen-year-old walls offset sinistrally 2.1 m by the Dead Sea transform, Israel. J. Geodyn. 24, 11–20.

Marco, S., Hartal, M., Hazan, N., Lev, L., Stein, M., 2003. Archaeology, history and geology of the A.D. Seven hundred and forty nine earthquake, Dead Sea transform. Geology 31 (8), 665–668.

Mart, Y., 1994. The Dead Sea rift, a leaky transform fault or an oblique spreading center: a short review. Africa Geosci. Rev. 1, 567–578.

Mart, Y., Dauteuil, O., 2000. Analogue experiments of propogation of oblique rifts. Tectonophysics 316, 121–132.

Mart, Y., Horowitz, A., 1981. The tectonics of the Timna region in Southern Israel and the evolution of the Dead Sea rift. Tectonophysics 79, 165–199.

Mart, Y., Ryan, W.B.F., Lunina, O.V., 2005. Review of the tectonics of the Levant Rift System: the structural significance of oblique continental breakup. Tectonophysics 395, 209–232.
Mart, Y., Rabinowitz, P.D., 1986. The northern Red Sea and the Dead Sea Rift. Tectonophysics 124, 85–113.
McClay, K.R., White, M.J., 1995. Analogue modeling of orthogonal and oblique rifting. Mar. Petrol. Geol. 12, 137–151.
Nikolaev, P.N., 1992. Methods of Tectonodynamics Analysis. Nedra Press, Moscow (in Russian).
Pavlides, S., Mountrakis, D.M., 1987. Extensional tectonics of northwestern Macedonia, Greece, since the Late Miocene. J. Struct. Geol. 9 (4), 385–392.
Picard, L., 1987. The Elat (Aqaba), Dead Sea, Jordan subgraben system. Tectonophysics 141, 23–32.
Picard, L.Y., Golani, U., Bentor, Y.K., Vroman, A., Zak, I., 1965. Israel geological map. Survey of Israel, scale 1:250,000 (reprinted in 1999).
Price, N.J., Cosgrove, J.W., 1990. Analysis of Geological Structures. Cambridge University Press.
Riznichenko, Yu.V., 1976. Dimensions of earthquake center and seismic momemt. In: Investigations on Physics of Earthquakes. Nauka Press, Moscow, pp. 9–27 (in Russian).
San'kov, V., Miroshnichenko, A., Levi, K., Lukhnev, A., Melnikov, A., Delvaux, D., 1997. Cenozoic stress field evolution in the Baikal rift zone. Bull. Centre Rech. Elf. Explor. Prod. 21, 435–455.
Sagy, A., Reches, Z., 2000. Fault pattern, joint systems and slip partitioning along the western margins of the Dead Sea rift. Dead Sea. In: Abstracts of the first Stephan Mueller Conference, Europe Geophysical Society, p. 34.
Scott, S.D., Benes, V., 1996. Oblique rifting in the Havre Trough and its propagation into the continental margin of New Zealand: comparison with analogue experiments. Marine Geophys. Res. 18, 189–201.
Shapira, A., 1997. On the seismicity of the Dead Sea basin. In: Niemi, T.M., Ben-Avraham, Z., Gat, J.R. (Eds.), The Dead Sea, the Lake and its Setting. Oxford University Press, pp. 82–86.
Sherman, S.I., Dneprovsky, Yu.I., 1989. Crustal Stress Fields and Geological and Structural Methods. Nauka Press, Novosibirsk (in Russian).
Sherman, S.I., Gladkov, A.S., 1999. Fractals in studies of faulting and seismicity in the Baikal Rift Zone. Tectonophysics 308, 133–142.
Sneh, A., 1996. The Dead Sea Rift: lateral displacement and downfaulting phases. Tectonophysics 263, 277–292.
Sneh., A., Bartov, Y., Weissbrod, T., Rosensaft, M., 1998. Geological map of Israel. Geological Survey of Israel, scale 1:200,000.
Tron, V., Brun, J.-P., 1991. Experiments on oblique rifting in brittle-ductile systems. Tectonophysics 188, 71–84.
Turcotte, T., Arieh, E., 1988. Catalogue of earthquakes in Esrael and adjacent areas. Appendix 2.5A of the Preliminary Safety Analysis Report, Israel Electric Company.
Turcotte, D.L., 1989. Fractal in geology and geophysics. Pure Appl. Geophys. 131, 171–196.
Twiss, R.J., Moores, E.M., 1992. Structural Geology. W.N. Freeman and Company Press, New York.
Van Eck, T., Hofstetter, R., 1990. Fault geometry and spatial clustering of microearthquakes along the Dead Sea-Jordan rift fault zone. Tectonophysics 180, 15–27.
Withjack, M.O., Jamison, W.R., 1986. Deformation produced by oblique rifting. Tectonophysics 126, 99–124.
Zilberman, E., Amit, R., Heimann, A., Porat, N., 2000. Changes in Holocene Paleoseismic activity in the Hula pull-apart basin, Dead Sea Rift, Northern Israel. Tectonophysics 321, 237–252.